Applying the Direct Bayesian Admissible Region Approach to The Association of GEO Belt Optical Observations

By Kohei FUJIMOTO[1)], Daniel J. SCHEERES[1)], Johannes HERZOG[2)], and Thomas SCHILDKNECHT[2)]

[1)] *The University of Colorado at Boulder, Boulder, Colorado, USA*
[2)] *The Astronomical Institute of the University of Bern, Bern, Switzerland*

The direct Bayesian admissible region approach is an a priori state free measurement association and initial orbit determination technique for optical tracks. In this paper, we test a hybrid approach that appends a least squares estimator to the direct Bayesian method on measurements taken at the Zimmerwald Observatory of the Astronomical Institute at the University of Bern. Over half of the association pairs agreed with conventional geometric track correlation and least squares techniques. The remaining pairs cast light on the fundamental limits of conducting tracklet association based solely on dynamical and geometrical information.

Key Words: Space Situational Awareness, Too-Short Arc Problem, Measurement Association, Initial Orbit Determination, Admissible Region

Nomenclature

RA, α	:	right ascension
DEC, δ	:	declination
a	:	semi-major axis
e	:	eccentricity
i	:	inclination
Ω	:	right ascension of the asc. node
ω	:	argument of periapsis
M	:	mean anomaly
ρ	:	range
$\dot{\rho}$	:	range-rate
ϕ	:	latitude of observatory
Θ	:	longitude of observatory
$\mathcal{C}$	:	criteria of the admissible region
A	:	support of the admissible region
$\mathcal{X}$	:	state space
t, τ	:	time
$F_{\mathcal{C}}$	:	admissible region for criteria $\mathcal{C}$
$\mathbf{X}$	:	state vector
$\mathfrak{Y}$	:	attributable vector
E	:	specific energy
$r_{\mathrm{a}}, r_{\mathrm{p}}$	:	orbit radius at apoapsis, periapsis
f, g, h	:	probability density function (pdf)
$\mathcal{T}$	:	time transformation fcn. for pdfs
β_1	:	simple linear reg. slope parameter
$\mathfrak{l}, \mathfrak{L}, \mathfrak{g}, \mathfrak{G}, \mathfrak{h}, \mathfrak{H}$	:	Poincaré orbital elements
x, y, z	:	Cartesian position coordinates
RMS	:	root mean sum
p	:	p-value of hypothesis test
δt	:	time gap between observations

Superscripts and subscripts

0	:	at epoch
max	:	maximum
min	:	minimum

1 Introduction

In space situational awareness (SSA), the vast majority of observations of objects beyond low-Earth orbit are made by optical sensors, which measure a time history of angles called "tracklets" for a given object[1,2)]. The range and range-rate, however, remains largely unconstrained, and thus multiple tracklets must be combined in order to obtain a full 6-dimensional state estimate. For short-arc observations common in survey-type observations, this task is not trivial as a large subset of the state space is consistent with any given tracklet pair. Therefore, traditional initial orbit determination (IOD) techniques often perform poorly giving rise to false correlation results and unrealistic state estimates.

The direct Bayesian admissible region approach proposed by Fujimoto and Scheeres is an *a priori* state free measurement association and IOD technique[3)]. Given a tracklet, a compact region in the range / range-rate space is defined based on a set of physical constraints such that all likely and relevant orbits are contained within it. The admissible region (AR) is a uniform probability density function (pdf) whose support is the aforementioned compact set[4,5)]. Multiple ARs may be propagated to a common epoch and an *a posteriori* pdf computed based on Bayes' rule. Such a direct approach is feasible because the ARs are well approximated as 2-dimensional manifolds in a 6-dimensional space, making the problem sparse. Furthermore, from the Theory of General Position, two ARs do not intersect generically and thus a non-zero *a posteriori* pdf is, in almost all cases, indicative that their corresponding tracklets are associated. IOD is achieved by examining the domain of the *a posteriori* pdf. Therefore, the rationale for the measurement association and the IOD are separate, allowing for both processes to be robust to outliers without

the need for excessive parameter tuning.

In this paper, the above method is applied to optical observations of geosynchronous (GEO) belt objects taken at the Zimmerwald Observatory of the Astronomical Institute at the University of Bern (AIUB)[6]. The outline is as follows. First, the necessary background theory, including the direct Bayesian admissible region approach, is outlined (*Background*). Current observational and orbit determination capabilities at AIUB are introduced. Next, the "hybrid" approach is proposed, where the direct Bayesian results are passed to a least squares batch filter (*Method*). Finally, association results of this new algorithm are discussed (*Results*). It produces 20 association pairs, over half of which agrees with conventional geometric tracklet correlation and least squares techniques. The remaining pairs suggest new association possibilities as well as cast light on the fundamental limits of conducting tracklet association based solely on dynamical information.

2 Background

In this section, necessary concepts are introduced, such as the too-short arc problem and tracklet association with the direct Bayesian admissible region. Next, observation capabilities at AIUB as well as the current procedure to process observations are discussed.

2.1 The Too-Short Arc Problem

Optical observations of resident space objects (RSOs) only contain angular information regarding the observed objects' states; that is, per observation, the range and range-rate remain largely unconstrained. Consequently, orbit determination has traditionally been conducted with some type of batch or sequential estimation algorithm, whose *a priori* information is supplied via geometric techniques known as initial orbit determination (IOD)[7,8]. Here, the association of observations must be assumed initially and then deduced from the quality of the least-squares fit; that is, the association of observations is a direct function of the quality of the orbit estimation and vice versa. This approach becomes problematic especially in a survey-type observation strategy. Usually, only a limited number of observations are available per night per object, each over short observation arcs, or *tracklets*, that span a few minutes[4]. Given such a small window of data, a large subset of the state space remains consistent with each tracklet, leading to poor convergence to the true solution if not divergence. The association of tracklets, therefore, cannot be inferred confidently.

Figure 1 shows the time history of the residuals in the angular variables when fitting two tracklets of a geostationary (GEO) satellite to its true state (Object 1) as well as a fictitious state (Object 2) separated by at least 270 km but still consistent with the observations. Table 1 shows the root mean sum (RMS) of the residuals. Each tracklet spans 2 minutes and consists of 5 observations; the two tracklets are separated by 20 minutes. A 2 arcsec 1-σ Gaussian noise is added to the observed angles. The Keplerian orbit elements (a [km], e, i [deg], Ω [deg], ω [deg], M [deg]) for each object at the simulation epoch is as follows:

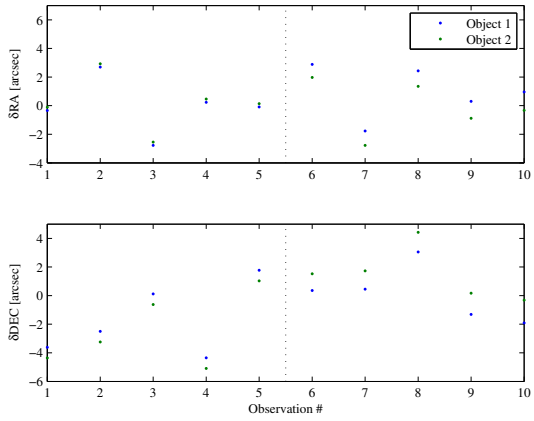

Figure 1: History of residuals in right ascension (δRA) and declination (δDEC) for simulated observations of a GEO object fit to its true state (Object 1) and a consistent but false state (Object 2).

	Object 1	**Object 2**
δRA [arcsec]	1.83405	1.72122
δDEC [arcsec]	2.37513	2.86219

Table 1: The RMS of the residuals in right ascension (δRA) and declination (δDEC) for simulated observations of a GEO object when fit to its true state (Object 1) and a consistent but false state (Object 2).

Object 1 $(42164.154, 10^{-6}, 0.1, 0, 0, 0)$

Object 2 $(41079.037, 0.01965, 0.1060, \ldots$
$-18.29, -161.8, -179.9)$.

We find that, in this situation, the residuals give us no indication which state is more likely.

Furthermore, in order to derive tractable geometric relationships between line-of-sight vectors, a simplistic dynamical model must be incorporated in the IOD. For example, the orbit may be assumed to be circular or the Earth's gravity field may be considered as a point mass[9]. The former fails to incorporate eccentric orbits such as those in a geostationary transfer orbit (GTO) or high area-to-mass ratio (HAMR) objects[10]. The latter, although valid for celestial bodies that are predominantly influenced by gravity, is less effective for RSOs which experience many perturbing forces including atmospheric drag, irregularities of the central body, and solar radiation pressure, just to name a few.

These difficulties in the association of optical tracklets of RSOs as well as the subsequent orbit determination are

referred to as the *too-short arc* (TSA) problem[2]. A similar problem, albeit in longer time scales, has been studied for heliocentric orbits; in fact, the method discussed in this paper was originally devised for the astrometry of celestial bodies[11,12]. The more general problem of multiple target tracking using bearing-only sensors continues to be tackled in the filtering community, but most solutions require a reference state, a Gaussian assumption on the error distribution, or great computational power[13,14].

2.2 The Direct Bayesian Admissible Region Apporoach

Various methods applying the *admissible region* (AR) concept to the TSA problem for RSOs have been studied in recent years[2,4,5,15]. In this paper, we define the AR as a pdf constrained in the range ρ and range-rate $\dot{\rho}$ directions via a few physical criteria such as that the orbit is elliptic, the object's range is within the sensing capabilities, and so on[3]. The angle and angle-rate, nominally in right ascension α and declination δ, at the epoch of a tracklet may be estimated via a least-squares fit of the tracklet data to a polynomial model in time. These variables plus necessary parameters, such as the latitude ϕ and longitude Θ of the observation point, are referred to collectively as the *attributable vector*[4]. Thus, each point on the AR combined with the attributable vector corresponds one-to-one with a state that the observed object may have taken. Furthermore, the covariance from the least-squares fit may be incorporated in the AR to represent observational errors.

Suppose that, given some set of criteria $\mathcal{C}$, A is a compact set in state space $\mathcal{X}$ that meet $\mathcal{C}$. Then, the AR $F_{\mathcal{C}}[\mathbf{X}(t^0);\mathfrak{Y}^0]$ is a pdf over $\mathcal{X}$ assigned to an attributable vector $\mathfrak{Y}^0$ such that the probability p that the observed object exists in region $B \subset A$ at time t^0 is

$$p[\mathbf{X}(t^0)] = \int_B F_{\mathcal{C}}[\mathbf{X}(t^0);\mathfrak{Y}^0]\mathrm{d}X_1^0\mathrm{d}X_2^0\ldots\mathrm{d}X_n^0, \quad (1)$$

where $\mathbf{X}(t^0) \in \mathcal{X}$ and

$$\mathbf{X}(t^i) \equiv \mathbf{X}^i = (X_1^i, X_2^i, \ldots, X_n^i). \quad (2)$$

Note that we impose $\int_A F_{\mathcal{C}}[\mathbf{X}(t^0);\mathfrak{Y}^0]\mathrm{d}\mathbf{X}^0 = 1$. Figure 2 is an example of an AR; here, as well as in the main analysis of this paper, the criteria are

$$\mathcal{C} = \bigcap_{i=1}^{4} \mathcal{C}_i, \quad (3)$$

and

$$\mathcal{C}_1 = \{(\rho,\dot{\rho}) : E \leq 0\} \quad (4)$$
$$\mathcal{C}_2 = \{(\rho,\dot{\rho}) : 1.03 \leq \rho \leq 8.53, -5 \leq \dot{\rho} \leq 5\} \quad (5)$$
$$\mathcal{C}_3 = \{(\rho,\dot{\rho}) : 1.03 \leq r_p\} \quad (6)$$
$$\mathcal{C}_4 = \{(\rho,\dot{\rho}) : r_a \leq 15\}. \quad (7)$$

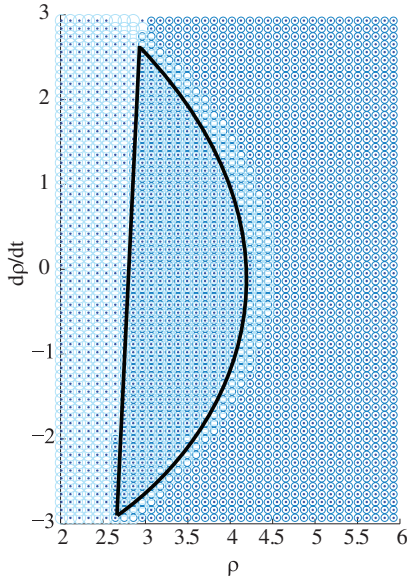

Figure 2: An admissible region for attributable vector $\mathfrak{Y} = (\alpha,\ \delta,\ \dot{\alpha},\ \dot{\delta},\ \phi,\ \Theta) =$ (118.26 deg, -13.62 deg, 29.06 arcsec/sec, 3.75 arcsec/sec, 5.73 deg, 275.02 deg).

where E is the specific geocentric energy of the particle, and r_a and r_p are the apoapsis and periapsis radii of the orbit, respectively. Units of length are in Earth radii and time in hours. The different shadings represent the different regions which satisfy each criterion in set $\mathcal{C}$; thus, the admissible region is where all types of shading overlap, or the region outlined by the black line. These criteria ensure that the AR encompasses most trackable object relevant to SSA while simultaneously filtering out highly eccentric orbits. Note that changing $\mathcal{C}$ allows one to be explicit about the types of orbits that are included in the analysis. For example, if the observer is only interested in surveying objects in and near the GEO belt, $\mathcal{C}$ may be modified to

$$\mathcal{C}_1 = \{(\rho,\dot{\rho}) : E \leq 0\} \quad (8)$$
$$\mathcal{C}_2 = \{(\rho,\dot{\rho}) : 5 \leq \rho \leq 8, -1 \leq \dot{\rho} \leq 1\} \quad (9)$$
$$\mathcal{C}_3 = \{(\rho,\dot{\rho}) : 5 \leq r_p\} \quad (10)$$
$$\mathcal{C}_4 = \{(\rho,\dot{\rho}) : r_a \leq 8\}. \quad (11)$$

The AR expresses our *limited* knowledge regarding ρ and $\dot{\rho}$ which are not directly observed. In conventional filtering, pdfs of the observations only describe the error in the attributable vector and are realized in the state space as likelihoods. For underdetermined systems, the integral of the likelihood function over the state space is divergent as we gain no information from the observations in coordinate directions corresponding to the variables not directly observed. We realize, however, that knowledge in these directions is not completely *lacking* for many real-world systems as the likelihood function may suggest. That is, we may add physical constraints $\mathcal{C}$ to the observed object's state such that we define a compact pdf F still representative of all

relevant states.

As a result, we may apply Bayes' rule directly to ARs in a common state space and at a common epoch τ; no reference state is required. To obtain the posterior pdf $h[\mathbf{X}(\tau)]$ based on two ARs $F_{\mathcal{C}}[\mathbf{X}^1;\mathcal{Y}^1]$ and $F_{\mathcal{C}}[\mathbf{X}^2;\mathcal{Y}^2]$,

$$h[\mathbf{X}(\tau)] = \frac{\{\mathcal{T}(\tau,t_1)\circ F_{\mathcal{C}}[\mathbf{X}^1;\mathcal{Y}^1]\}\{\mathcal{T}(\tau,t_2)\circ F_{\mathcal{C}}[\mathbf{X}^2;\mathcal{Y}^2]\}}{\int\{\mathcal{T}(\tau,t_1)\circ F_{\mathcal{C}}[\mathbf{X}^1;\mathcal{Y}^1]\}\{\mathcal{T}(\tau,t_2)\circ F_{\mathcal{C}}[\mathbf{X}^2;\mathcal{Y}^2]\}\mathrm{d}\mathbf{X}}, \quad (12)$$

where $\mathcal{T}(\tau,t^i)$ is a transformation that maps some pdf $f(\mathbf{X}^i,t^i)$ from time t^i to τ, and $\mathbf{X}(\tau)\equiv\mathbf{X}$. The domain of integration is over the entire state space. Note that, in general, any pdf may be used as input, such as density information from debris distribution models [16]. This approach is computationally feasible because each AR, ignoring observation errors, has codimension 4, making the problem extremely sparse. Furthermore, the sparseness also ensures that misassociations are highly unlikely unless the association is consistent with both the observation geometry and the dynamics [17]. From the Theorem of General Position, $h[\mathbf{X}(\tau)]=0$ for all $\mathbf{X}$ generically if

$$\dim\{F_{\mathcal{C}}[\mathbf{X}^1;\mathcal{Y}^1]\}+\dim\{F_{\mathcal{C}}[\mathbf{X}^2;\mathcal{Y}^2]\}<\dim(\mathcal{X}), \quad (13)$$

where $\dim(\mathcal{X})$ is the dimension of the state space. Again, ignoring observation errors, $\dim\{F_{\mathcal{C}}[\mathbf{X}^i;\mathcal{Y}^i]\}=2$ so the inequality holds for $\dim(\mathcal{X})>5$. The justification of associations is not at all related to the OD quality but rather solely by the geometry of the AR maps; therefore, this method is robust with minimal tuning.

Finally, transformation $\mathcal{T}(\tau,t^i)$ is expressed analytically by means of a special solution to the Fokker-Planck equations valid for all deterministic dynamical models. Given solution flow $\mathbf{X}(t)=\phi(t;\mathbf{X}^i,t^i)$ to the dynamics for initial conditions $\mathbf{X}^i$, the pdf $\mathcal{T}(\tau,t^i)\circ f(\mathbf{X}^i,t^i)=f(\mathbf{X},\tau)$ is expressed as

$$f(\mathbf{X},\tau)=f[\phi(\tau;\mathbf{X}^i,t^i),\tau]=f(\mathbf{X}^i,t^i)\left|\frac{\partial\mathbf{X}(\tau)}{\partial\mathbf{X}^i}\right|^{-1}, \quad (14)$$

where $|\cdot|$ indicates the determinant operator.

2.3 Observation Capabilities And Processing at AIUB

The Zimmerwald observatory, located about 10km south of Berne, Switzerland, consists of several optical telescopes [18–20]. One of them, the Zimmerwald SMall Aperture Robotic Telescope (ZimSMART), is best suited for surveying the sky searching for RSOs. ZimSMART is used to develop an orbital elements catalogue; a photograph is given in Figure 3 its specs are listed in Table 2. Two different orbital regions are surveyed: the GEO ring and the Medium Earth Orbit region (MEO). The aim of the surveys of the GEO ring is maximum coverage of the region around the celestial equator which can be observed from Zimmerwald.

Images taken with ZimSMART are analyzed as follows. First, the right ascension and declination (RA/DEC) of each

Figure 3: Current setup of ZimSMART [18].

RSO in the image files are automatically extracted. For each star, which appear streak-like, the center of mass is calculated. RSOs, on the other hand, appear point-like; their centers of mass are calculated as well. As each image has a finite exposure time, the epoch of the coordinates is chosen to be the mid-exposure time. The RA/DEC of the RSOs are calculated relative to celestial bodies whose physical coordinates are known and cataloged. If the same object is detected on at least 3 images, a *tracklet* will be produced; i.e., a text file containing the observing epoch, position in right ascension and declination, and apparent magnitude of the object for each image.

After extracting tracklets, one has to identify the observed objects. We perform this process in three steps. First, we correlate each tracklet with the JSpOC two-line element (TLE) catalogue and an internal AIUB catalogue via positions and velocities. The complete procedures are described in detail in Früh, et al [20]. In the second step, the leftover tracklets are tested pairwise to check if some of them belong to the same object; if so, they are stored as combined tracklets. Tracklets, for which no other fitting tracklet could be found, remain single. This procedure reduces the amount of computations in the following step. In the last step of the object identification process, the orbital elements of objects in the AIUB internal catalogue are compared with those of the new combined and single tracklets. This method is very effective for newly detected objects with observations from only one night. More details are described in Herzog, et al [19]. The identifications via positions and velocities as well as those via orbital elements have to be confirmed by a statistical orbit determination (OD). The new tracklet is associated with an internal catalog object only if the OD is successful; i.e., if the RMS of the residuals of a least squares batch filter is below 1.5 arcsec. Due to the tracklets being *too short arc* and lacking dynamical information, especially when the tracklet pairs span a single night, not every Keplerian element is included in the RMS,

Table 2: Instrument specs for the ZimSMART telescope.

Spec	**Value**
Lat., Long., Alt. [deg, deg, m]	46.8772 N, 7.4652 E, 951.2
Cartesian [m]	4331306.2000, 567553.9900, 4633121.6600
System	WGS-84
Telescope mount	ASA DDM85
Telescope tube	Takahashi ε-180
Aperture diameter	180 mm
Focal length	500 mm
Detector type	CCD
Detector size	4096 $\times$ 4096 pixel
Field of view	$2^\circ \times 2^\circ$
Typical readout time	7 s
Wavelengths	White light
Typical exposure time	10 s
Sensitivity	Magnitude 13.5 for 10s exposure time (1m objects in GEO)

but rather only the semi-major axis, inclination, and right ascension of the ascending node.

Surveys of the geostationary ring are executed by scanning declination stripes with fixed right ascension. These observations are taken without a priori information of any catalogue objects. For the survey from which data processed in this paper is extracted, 24 stripes are taken separated by 1 hour in right ascension. These stripes are at 0 hr, 1hr, . . . , 23 hr. Each stripe contains five fields separated in declination by the field of view, and similarly, five images are taken for each field. The declination of the lowest field depends on the known density of RSOs. The advantage of this method is that the observations can be acquired in a fully automated fashion with no human interaction. The telescope software chooses the visible fields automatically. Again, a tracklet contains a minimum of three images and a maximum of five, corresponding to the number of images taken per field. Depending on the exposure time and the number of images, a tracklet thus spans anywhere between $1 \sim 2$ minutes.

3 Method

In this section, we explain in detail how the direct Bayesian admissible region theory (c.f. Section 2.2) is corroborated with optical short-arc measurements of GEO and high Earth orbit (HEO) objects taken with the setup at AIUB (c.f. Section 2.3). We process a set of tracklets taken with the ZimSMART telescope over one RA fence; detailed measurement parameters are given in Table 3. The association and state estimation results are ultimately compared to those output by the current correlation scheme in Section 2.3.

When the direct Bayesian approach is applied to the tracklets with the nominal assumption that the observation errors are small enough to be ignored, one is faced with two difficulties. The first is that the ambiguity in the number of revolutions the observed object potentially made between two tracklet pairs leads to a large number of false associations. A theoretical explanation of these fictitious solutions, or *multi-rev* solutions, is given in Fujimoto and Scheeres[3)]. The second difficulty is that the zero-error assumption causes missed associations especially when the state space discretization is refined to improve estimation accuracy to practical levels[21)]. The extension of the two-dimensional linear map extrapolation proves to be too computationally expensive for this particular problem[22)].

We propose a hybrid approach that takes the tracklet association and initial orbit determination results of the direct Bayesian method and passes them to a least squares estimator. Although the steps in this new process are similar to those in a traditional IOD[23)], the justification of the association and the estimation are separated, thus improving robustness. Furthermore, in order to better exclude multi-rev solutions, a minimum limit $p_{\min}$ is set to the p-value associated with the model utility test of the observed minus computed ($O - C$) residuals. That is, if we let the simple linear regression slope parameter of the residuals be β_1, for the hypothesis test

$$\begin{cases} H_0 : \beta_1 = 0 \\ H_1 : \beta_1 \neq 0, \end{cases} \tag{15}$$

where H_0 is the null and H_1 the alternative hypothesis, the probability of falsely rejecting H_0 is set to be $p_{\min}$.

Table 3: Parameters for the data set used in this paper. # of objects detected is based on AIUB correlation results.

Parameter	**Value**
Epoch of Initial Field	Aug 18, 2012 22:59:08.64 UTC
Epoch of Final Field	Aug 20, 2012 02:01:32.69 UTC
Total # of Fields	55
Total # of Tracklets	212
Total # of Objects Detected	48
# of Objects Detected Twice w/ 24h Gap	19

Table 4: For two orbit estimates computed based on the hybrid approach, the semi-major axis (a), eccentricity (e) and inclination (i) are listed along with the RMS of the residuals for the first tracklet in RA ($\mathrm{RMS_{RA}}$) and the linear regression slope parameter ($\beta_{1,\mathrm{RA}}$) with its corresponding p-value.

	a **[km]**	e	i **[deg]**	$\mathbf{RMS_{RA}}$**[arcsec]**	$\boldsymbol{\beta_{1,\mathrm{RA}}}$	p
Solution 1	20285	0.57013	2.2261	0.24841	0.97512	0.00469
Solution 2	42166	0.00466	0.2886	0.05599	-0.13651	0.82673

Through this step, a maximum bound is effectively set for β_1 itself, meaning the residuals must be unrelated to time in a linear sense for a tracklet pair to be associated to a state estimate. $\beta_1 = \pm 1$ iff all sample pairs lie on a straight line; thus, although it is not always the case that $\beta_1 = 0$ if the residuals are unrelated to time, since the tracklets arcs are so short, it is assumed that the residual bias is linear enough for one to use slope parameter β_1 in this context[24].

We now present an outline of the hybrid algorithm. First, the time history of right ascension and declination must be converted into an attributable vector at the tracklet epoch; i.e. a single set of angles and angle-rates. The measured angles are fit to a polynomial kinematic model in time, such as for the right ascension

$$\alpha(t) = \alpha^0 + \dot{\alpha}^0(t - t^0) + \frac{1}{2}\ddot{\alpha}^0(t - t^0)^2, \qquad (16)$$

where superscript 0 denotes the state at the tracklet epoch[4]. Next, admissible regions are computed for each attributable vector in the Poincaré orbit element space ($\mathfrak{L}$, $\mathfrak{l}$, $\mathfrak{G}$, $\mathfrak{g}$, $\mathfrak{H}$, $\mathfrak{h}$), which are a canonical counterpart to equinoctial elements[8]. They are defined with respect to the Keplerian orbit elements as follows:

$$\begin{aligned}
\mathfrak{l} &= \Omega + \omega + M \\
\mathfrak{L} &= \sqrt{\mu a} \\
\mathfrak{g} &= \sqrt{2\mathfrak{L}\left(1 - \sqrt{1 - e^2}\right)}\cos(\omega + \Omega) \\
\mathfrak{G} &= -\mathfrak{g}\tan(\omega + \Omega) \\
\mathfrak{h} &= \sqrt{2\mathfrak{L}\sqrt{1 - e^2}\,(1 - \cos i)}\cos\Omega \\
\mathfrak{H} &= -\mathfrak{h}\tan\Omega,
\end{aligned} \qquad (17)$$

where μ is the standard gravitational parameter. As discussed in Fujimoto and Scheeres[3], the admissible region is divided into 375,000 subsets (750 units of discretization in the range-direction $\times$ 500 units in the range-rate) and each subset linearly extrapolated. The Poincaré space, and consequently ARs, are discretized such that the bounds of the state space are

$$\mathbf{X}_{\min} = (4.5285, 0, -3, -3, -4, -4) \qquad (18)$$

$$\mathbf{X}_{\max} = (14.110, 6.2832, 3, 3, 4, 4), \qquad (19)$$

where the units are in Earth radii - kg - hr. The bin size is set such that the sides are $1.1052 \cdot 10^{-2}$ ($\mathfrak{L}$), $1.7453 \cdot 10^{-2}$ ($\mathfrak{l}$), $1.6667 \cdot 10^{-2}$ ($\mathfrak{G}$, $\mathfrak{g}$), and $2.2222 \cdot 10^{-2}$ ($\mathfrak{H}$, $\mathfrak{h}$) for a total of 5.2424×10^{15} bins over the entire space. This resolution corresponds to approximately 100 km in the semi-major axis direction and 1 degree in the mean anomaly direction. The admissible region are propagated to a common epoch, which is chosen to be the tracklet epoch of the first tracklet, under two-body dynamics. The two-body assumption is made only to simplify the problem and is not central to the direct Bayesian technique.

To avoid the high computational cost of all-on-all association, the posterior pdf $h[\mathbf{X}(\tau)]$ based on the admissible regions is computed for tracklet pairs in reverse chronological order (i.e., for a set of N tracklets ordered by epoch, Tracklet 1 + Tracklet N, Tracklet 1 + Tracklet $N-1$, ...) until we find a pair for which $h[\mathbf{X}(\tau)] > 0$[3]. We then temporarily claim these tracklets as associated and run a bank of least squares filters simultaneously to refine the fit of the measurements to the state estimate. Note that if an object catalogue exists, then one should first correlate tracklets with these objects first. Also, only tracklet pairs whose epochs are separated by at least 24 hours are considered so that enough dynamical information is available.

The reference state of each filter is the centroid of each

bin where $h[\mathbf{X}(\tau)] > 0$ transformed into the J2000 cartesian space. In this paper, we assume that no *a priori* information exists; if desired, the *a priori* covariance may be set to approximate $h[\mathbf{X}(\tau)]$. The assumed observation error is set to 2 arcsec 1-σ. The observation-state relationship and corresponding linear partials matrix assume a spherical Earth

$$x = \rho \cos\alpha \cos\delta \tag{20}$$

$$y = \rho \sin\alpha \cos\delta \tag{21}$$

$$z = \rho \sin\delta. \tag{22}$$

For the set of filters that converge, if

1. the root mean sum (RMS) of the $O - C$ residuals for both RA and DEC over all tracklets processed is less than some maximum $\mathrm{RMS}_{\max}$ AND

2. the p-value of the model utility test for both the RA and DEC for each individual tracklet is greater than some minimum $p_{\min}$,

then the tracklets are confirmed to be associated and the state estimate with the smallest $O - C$ residual RMS is added to the object catalogue. In this paper, $\mathrm{RMS}_{\max} = 0.7$ arcsec and $p_{\min} = 0.1$; these values are chosen to best describe the observational capabilities of ZimSMART. Finally, the next tracklet in the set is paired with other tracklets as before, and the process is repeated until all tracklets are processed.

As an example of how the linear regression slope parameter can help identify multi-rev solutions, Table 4 shows the association result of two tracklets correlated with the current AIUB approach to object 98006B in the JSpOC TLE catalog. For Solution 1, which is most likely a multi-rev solution, even though the RMS of the residuals in RA over the first tracklet is smaller than the gating criterion, the β_1 value suggests a strong linear relationship between the residuals over time. In addition, the small p-value indicates that it is highly unlikely to falsely infer $\beta_1 \neq 0$ due to random chance.

4 Results

In this section, the outcome of tracklet association via the hybrid approach outlined in Section 3 is discussed. The observation strategy is described in Section 2.3. Table 5 is a table of all 20 associated tracklet pairs detected. The solutions can be categorized into three types. **Type I** solutions (11/20 = 55% of solutions) agree with the correlation and association results of existing code at AIUB. **Type II** solutions (7/20 = 35%) associate two tracklets which AIUB code determined belongs to two separate objects. **Type III** solutions (2/20 = 10%) include at least one tracklet which the AIUB code did not correlate or associate. We examine in detail the 45% of solutions that did not agree with existing techniques.

Table 5: Summary of association results ordered by solution type. Tracklets correlated to the JSpOC TLE catalog objects are indicated by the object's 6 letter international designator. Tracklets associated with objects in AIUB's internal catalog are indicated by the object's 7 letter designator starting with "Z." Tracklets newly associated are indicated by a bracketed number assigned by tracklet epoch.

Type	Object ID	Tracklet #1	Tracklet #2	δt [days]
Type I	2	'94022A'	'94022A'	1.01325
	3	'93078B'	'93078B'	1.00508
	5	'00081A'	'00081A'	1.00508
	11	'91075A'	'91075A'	1.00387
	12	'02015B'	'02015B'	1.00172
	13	'98006B'	'98006B'	1.00172
	14	'10025A'	'10025A'	1.00172
	15	'08034B'	'08034B'	1.00172
	16	'98057A'	'98057A'	1.00172
	17	'85015B'	'85015B'	1.01285
	19	'Z11003C'	'Z11003C'	1.00932
Type II	4	'10032B'	'98050A'	1.00635
	6	'98050A'	'09008B'	1.08071
	7	'00054A'	'10025A'	1.00635
	9	'08065B'	'10021A'	1.01453
	10	'11041A'	'98057A'	1.00603
	18	'04008A'	'98024A'	1.03621
	20	'01042A'	'Z12230G'	1.00963
Type III	1	[3]	'Z12230C'	1.00635
	8	[13]	[120]	1.00635

4.1 Type II Solutions

Table 6 lists the semi-major axis, eccentricity, and inclination of the Type II solutions. We find that none of the objects are at GEO altitude; in fact, all objects except for Object 6 are in altitudes where it is unlikely that any objects exist. As can be inferred from the strict gating required for an association to be detected ($\mathrm{RMS}_{\max} = 0.7$ arcsec), however, these are not degenerate solutions but rather multi-rev solutions that arise from the ambiguity of the number of revolutions made by the observed object during the observation gap. Indeed, if we are to look at ratio of the time gap between tracklets to the orbital period of the solution, they are all nearly integers between 1 and 3.

Figures 4 and 5 are graphical representations of Object 9 as well as the two catalogued objects to which the AIUB code correlated. As expected, Object 9 and the catalogued objects align along the observation direction at each tracklet epoch. We find that the slight inclination common to Type II solutions is necessary so that the solution appears at the same declination as an object in the GEO ring.

4.2 Type III Solutions

Table 7 lists the Keplerian orbital elements of the Type III solutions found and Figure 6 is a plot of their groundtracks. Unlike the Type II solutions, both objects are very

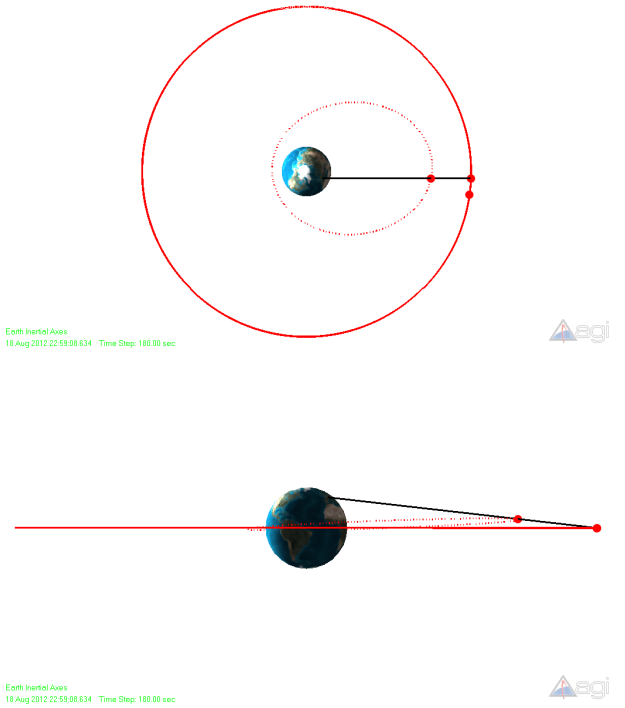

Figure 4: The orbit (dotted red line) and position of Object 9 at the first tracklet epoch along with orbits and positions of catalogued objects 08065B and 10021A (solid red lines) as well as the observation direction (black). Figures generated with AGI's STK.

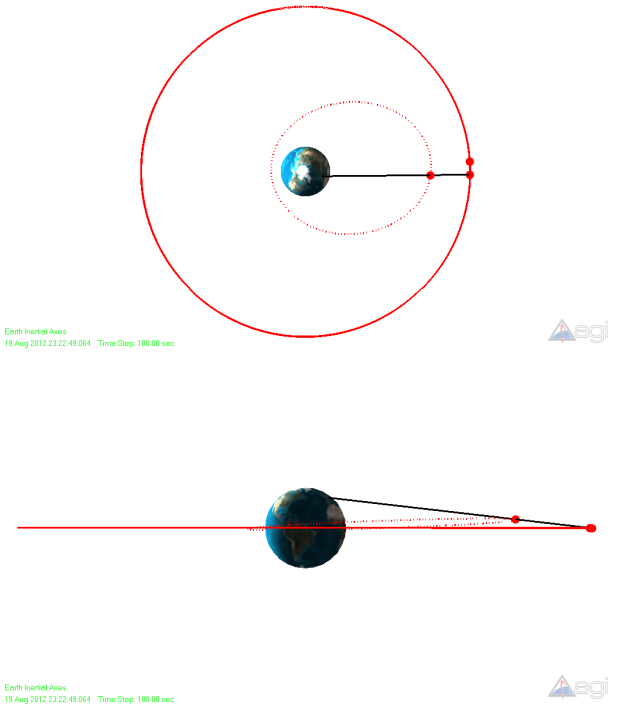

Figure 5: Similar to Figure 4 but for the second tracklet epoch. Figures generated with AGI's STK.

near circular at geosynchronous altitude, making it likely that they are uncatalogued objects. Here, the long time gap between tracklets allowed the admissible regions to dynamically evolve so that previously uncorrelated tracks could be linked together.

4.3 Potential Improvements of The Observation Strategy

The proposed idea of applying a least squares batch filter to the direct Bayesian probabilistic output is effective but nonetheless can still be improved. Table 8 sorts the 19 objects expected to be detected based on the AIUB correlation results by whether it matches the results from the hybrid method or not. Type II solutions are not completely rejected; consequently, about 15% of the expected objects are missed due to one or more of their tracklets being associated to a multi-rev solution. Ruling out apparent multi-rev solutions as false associations given just the two tracklets and dynamical system flow may be difficult, especially when the measurement residuals are so well behaved. Note that multi-rev solutions are not a problem in the AIUB code as the tracklets are never associated beyond a single night. This approach is not ideal either; as discussed in Section 2.1, a lack of dynamical information can also lead to poor association solutions. Indeed, new objects within the GEO belt are detected with the hybrid approach where the associated tracklets are separated by at least 24 hours.

Table 6: For Type II solutions, listed here are the semi-major axis a, eccentricity e, inclination i, and ratio between the observation time gap δt and the orbit period T.

Object ID	a [km]	e	i [deg]	$\delta t/T$
4	20370.27	0.574014	2.36898	3.001
6	44103.76	0.033165	0.15711	1.013
7	20367.00	0.601097	4.21171	3.002
9	20489.57	0.566496	2.53346	2.999
10	26695.54	0.385897	1.64413	2.000
18	27240.55	0.344950	0.95749	2.001

The easiest way to reject multi-rev solutions is to conduct follow-on observations based on the estimated state. If the multi-rev solution is indeed truth, then its short orbital period relative to GEO objects should allow it to be observed multiple times per night. Alternatively, one can make better use of the information already available in the observations. Geometric correlation to JSpOC catalogued objects as implemented in the current AIUB code is, in effect, one example where *a priori* information is fused into the association process. Preconditioning the ARs with pdfs derived from debris catalogues or density models may similarly be effective; the prior has been implemented in previous work to greatly improve computational speed[3]. Information which would allow one to distinguish between tracklets also exists outside of the realm of dynamics, such as photometry and spectroscopy from the CCD image files[25–27]. Finally, be-

Table 7: For Type III solutions, listed here are all 6 Keplerian orbital elements: semi-major axis a, eccentricity e, inclination i, right ascension of the ascending node Ω, argument of periapsis ω, and mean anomaly M.

Object ID	a **[km]**	e	i **[deg]**	Ω **[deg]**	ω **[deg]**	M **[deg]**
1	42167.94	0.005040	8.74794	38.5298	38.449	264.763
8	42166.74	0.000314	0.09691	56.8309	143.201	140.752

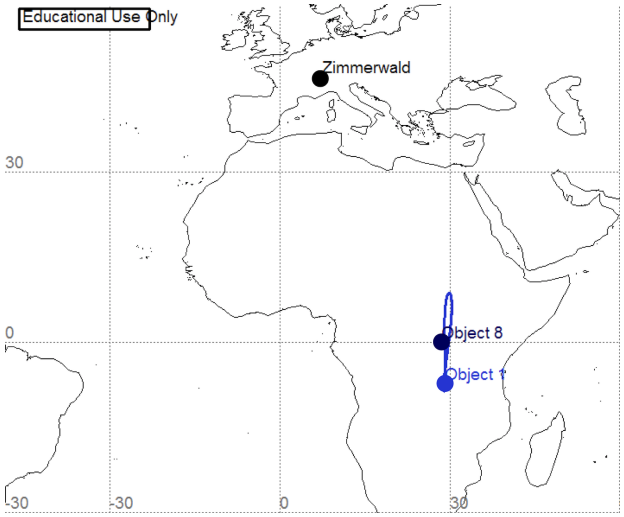

Figure 6: Ground tracks of Type III solutions for a full orbit from the tracklet epoch: Objects 1 (light blue) and 8 (dark blue). The position of each object at the epoch of the first tracklet is indicated by a dot. The position of the Zimmerwald observatory is also plotted with a black dot. Figure generated with AGI's STK.

cause the evaluation of Bayes' rule when associating ARs is an embarrassingly parallel problem, all-on-all association may be possible within a reasonable time if many computation cores are available.

Additionally, about 25% of the 19 expected objects are completely missed by the hybrid approach. The solution corresponding to object 82082A is rejected due to a particularly large $O - C$ residual value (-2.445 arcsec) in the declination direction for one angle measurement. If this particular measurement is excluded, the RMS of the declination residuals improves from 1.0113 arcsec to 0.59865 arcsec: within the maximum RMS gate for this paper. For all of the other solutions, the p-value limit for the model utility test of the residuals is triggered most probably by mistake. Figure 7 is one such example: the residuals in the declination direction for the first tracklet is "linear enough" such that $p = 0.0432 < p_{\min} = 0.1$. As such, there exist observation scenarios where reliably evaluating the "no linear relationship" null-hypothesis can be difficult due to the small number of individual angle measurements included in a tracklet. Increasing measurements per tracklet not only will shed better light on any biases present in the residuals but also has the added benefit of improving the angle-rate estimate in the attributable vector.

Table 8: Objects where multiple tracklets with at least a 24 hour time gap are correlated based on the AIUB algorithm. Tracklets of objects under "Agreement" are associated similarly with the hybrid approach, "multi-rev" associated with another object, and "missed" not associated at all. Number of objects in each category in parenthesis.

Agreement (11)	**Multi-Rev (3)**	**Missed (5)**
00081A		
02015B		
08034B		
10025A		
85015B		
91075A		
93078B		82082A
94022A		84028A
98006B	00054A	93015A
98057A	11041A	95067A
Z11003C	98050A	98056A

Because the theory discussed in this paper addresses the TSA problem in a much more probabilistically straightforward way than other IOD techniques, it allows one to reevaluate future observational strategies so that they minimize false positive / negative association solutions. Any changes to the current strategy, such as the time gap between tracklets, directly affects the *a posteriori* pdf in the state space without the need to assume an observation geometry, dynamical system, or type of errors accounted for. Furthermore, it is not necessary to parametrically account for multi-rev solutions, which explained all false positive solutions encountered in this paper; rather, they naturally appear in the *a posteriori* pdf as long as they are dynamically viable.

5 Conclusions

In this paper, the direct Bayesian admissible region approach to short-arc association and initial orbit determination is applied to optical observations taken at the Astronomical Institute of the University of Bern. Traditional methods rely on the quality of the orbit determination to conduct observation association, which is often unreliable. The direct Bayesian approach improves robustness by leveraging the sparseness of probability distributions that describe range and range-rate ambiguity given a single

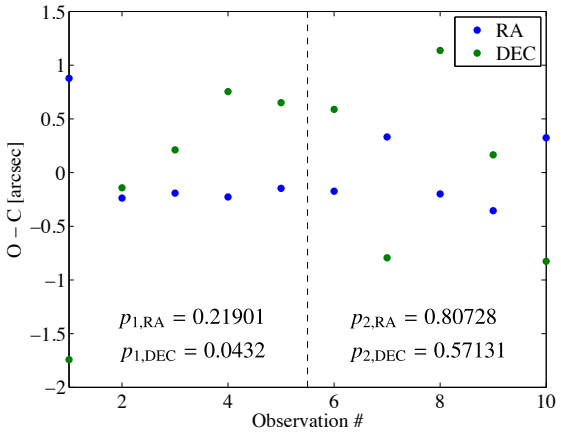

Figure 7: History of RA/DEC $O-C$ residuals using the hybrid method for two tracklets correlated to object 84028A with current AIUB code. Plot points to the left of the dotted line are for the first tracklet and to the right the second. p-values for the model utility test are indicated per tracklet and angle.

optical track. Furthermore, a hybrid approach that appends a least squares batch filter is found to efficiently incorporate measurement error and reduce false positives due to multi-rev solutions. Processing a set of 212 tracklets resulted in 20 objects detected; 2 of which are newly detected by the proposed method. Nonetheless, about 35% of the solutions are still deemed to be false positive solutions, and thus ideas to further reject multi-rev solutions are proposed. Future work is to implement these ideas, such as increasing the number of angle measurements per tracklet, as well as further testing of the hybrid approach with more data sets.

References

1) K. J. DeMars, M. K. Jah, and P. W. Schumacher. The use of short-arc angle and angle rate data for deep-space initial orbit determination and track association. 2009. Presented at the Eighth US/Russian Space Surveillance Workshop, Wailea-Maui, HI.
2) G. Tommei, A. Milani, and A. Rossi. Orbit determination of space debris: admissible regions. *Celestial Mechanics and Dynamical Astronomy*, 97:289–304, 2007.
3) K. Fujimoto and D. J. Scheeres. Correlation of optical observations of earth-orbiting objects and initial orbit determination. *Journal of Guidance, Control, and Dynamics*, 35(1):208–221, 2012.
4) J. M. Maruskin, D. J. Scheeres, and K. T. Alfriend. Correlation of optical observations of objects in earth orbit. *Journal of Guidance, Control and Dynamics*, 32(1):194–209, 2009.
5) K. J. DeMars and M. K. Jah. Initial orbit determination via gaussian mixture approximation of the admissible region. 2012. Presented at the AAS/AIAA Spaceflight Mechanics Meeting, Charleston, SC, AAS 12-260.
6) T. Schildknecht, W. Flury, C. Früh, J. Herzog, A. Hinze, and A. Vananti. Using optical observations to survey, track, and characterize small-size objects at high altitudes. 2011. Presented at the 28th International Symposium on Space Technology and Science, Okinawa, Japan, 2011-r-07.
7) B. D. Tapley, B. E. Schutz, and G. H. Born. *Statistical Orbit Determination*. Elsevier Academic Press, Burlington, MA, 2004. pp. 159-284.
8) D. Vallado. *Fundamentals of Astrodyamics and Applications*. Microcosm Press, Hawthorne, CA, third edition, 2007.
9) C. Früh, T. Schildknecht, R. Musci, and M. Ploner. Catalogue correlation of space debris objects. In *5th European Conference on Space Debris*, 2009.
10) A. Rosengren and D. Scheeres. Long-term dynamics of HAMR objects in HEO. 2012. Presented at the *AIAA/AAS Astrodynamics Specialist Conference*, Minneapolis, Minnesota, AIAA 2012-4745.
11) A. Milani, G. Gronchi, M. Vitturi, and Z. Knežević. Orbit determination with very short arcs. i admissible regions. *Celestial Mechanics and Dynamical Astronomy*, 90:57–85, 2004.
12) A. Milani and Z. Knežević. From astrometry to celestial mechanics: orbit determination with very short arcs. *Celestial Mechanics and Dynamical Astronomy*, 92:118, 2005.
13) D. R. Reid. An algorithm for tracking multiple targets. *IEEE Transactions on Automatic Control*, AC-24(6):843–854, 1979.
14) F. Gustafsson, F. Gunnarsson, N. Bergman, U. Forssell, J. Jansson, R. Karlsson, and P. Nordlund. Particle filters for positioning, navigation, and tracking. *IEEE Transactions on Signal Processing*, 50(2): 425 – 437, 2002.
15) D. Farnocchia, G. Tommei, A. Milani, and A. Rossi. Innovative methods of correlation and orbit determination for space debris. *Celestial Mechianics and Dynamical Astronomy*, 107(1-2):169–185, 2010.
16) M. Oswald, S. Stabroth, C. Wiedemann, P. Wegener, H. Klinkrad, and P. Vörsmann. ESA's MASTER 2005 debris environment model. *Advances in the Astronautical Sciences*, 123(1):811–824, 2006.
17) J. S. Carter. *How Surfaces Intersect in Space: An introduction to topology*. World Scientific, Singapore, second edition, 1995. pp. 277.
18) J. Herzog, T. Schildknecht, and M. Ploner. Space debris observations with ZimSMART. 2011. Presented at the *European Space Surveillance Conference*, Madrid, Spain.
19) J. Herzog, C. Früh, and T. Schildknecht. Build-up and maintenance of a catalogue of GEO objects with ZimSMART and ZimSMART 2. 2010. Presented at the *61st International Astronautical Congress*, Prague, Czech Republic. IAC-10.A6.5.2.
20) C. Früh, T. Schildknecht, R. Musci, and M. Ploner. Catalogue correlation of space debris objects. 2009. Presented at the *Fifth European Conference on Space Debris*, Darmstadt, Germany.
21) K. Fujimoto and D. J. Scheeres. Applications of the admissible region to space-based observations. 2011. Presented at the 2011 AAS/AIAA Astrodynamics Specialist Conference, Girdwood, AK. AAS-11-574.
22) K. Fujimoto and D. J. Scheeres. Non-linear bayesian orbit determination: Angle measurements. 2012. Presented at the *63rd International Astronautical Congress*, Naples, Italy. IAC-12-C1.6.11.
23) G. Beutler. *Methods of Celestial Mechanics Volume I: Physical, Mathematics, and Numerical Principles*. Astronomy and Astrophysics Library. Springer-Verlag, Berlin, Germany, 2005.
24) J. L. Devore. *Probability and Statistics for Engineering and the Sciences*. Wadsworth Publishing Company, Belmont, CA, USA, 4th edition, 1995.
25) R. L. Scott and B. Wallace. Small-aperture optical photometry of Canadian geostationary satellites. *Can. Aeronaut. Space J.*, 55(2): 41–53, 2009.
26) T. Schildknecht, A. Vananti, H. Krag, and C. Erd. Reflectance spectra of space debris in GEO. 2009. Presented at the *Advanced Maui Optical and Space Surveillance Technologies Conference*, Wailea-Maui, HI.
27) T. Schildknecht, C. Früh, J. Herzog, A. Hinze, and A. Vananti. AIUB efforts to survey, track, and characterize small-size objects at high altitudes. 2010. Presented at the *Advanced Maui Optical and Space Surveillance Technologies Conference*, Wailea-Maui, HI.